International Journal of Quantum Chemistry

Path integral Monte Carlo calculations of calcium-doped ^{4}He clusters

Journal:	*International Journal of Quantum Chemistry*
Manuscript ID:	Draft
Wiley - Manuscript type:	Full Paper
Date Submitted by the Author:	n/a
Complete List of Authors:	Rodríguez-Cantano, Rocío; CSIC, Instituto de Física Fundamental Gonzalez-Lezana, Tomas; CSIC, Instituto de Fisica Fundamental Villarreal, Pablo; CSIC, Instituto de Física Fundamental López-Durán, David; CSIC, Instituto de Catálisis y Petroquímica Gianturco, Franco; Univ. Rome La Sapienza, Chemistry and CNISM Delgado-Barrio, Gerardo; CSIC, Instituto de Física Fundamental
Keywords:	Helium clusters, Path integral Monte Carlo

Path integral Monte Carlo calculations of calcium-doped ^{4}He clusters

R. Rodríguez-Cantano*, T. González-Lezana*, P. Villarreal*, D. López-Durán†, F. A. Gianturco‡, and G. Delgado-Barrio*§

December 19, 2013

Abstract

The energetics and structures of $He_N Ca$ clusters have been studied by means of path integral Monte Carlo (PIMC) calculations. Sizes ranging between $N = 10$ and 40 helium atoms were considered at $T = 1$, 1.5 and 2 K. Radial and angular distributions have been analyzed in detail to investigate the geometry of the bound systems. The comparison of the results obtained with two current He–Ca interactions [Kleinekäthofer Chem. Phys. Lett., **2000**, 324, 40, and Lovallo *et al.*, J. Chem. Phys. **2004**, 120, 246] reveals substantial differences regarding the precise location of the Ca impurity with respect to the helium droplet. Whereas the use of the first potential yields a doped cluster in which the Ca atom is solvated inside a helium cage, predictions with the much weaker He–Ca potential by Lovallo *et al.* correspond to the formation of a dimple at the surface of the outer He atoms to host the Ca atom, a situation which is consistent with the experimental findings for the system.

*Instituto de Física Fundamental, IFF-CSIC, Serrano 123, 28006 Madrid, Spain
†Inst. de Catálisis y Petroleoquímica - CSIC, Marie Curie 2, Cantoblanco, 28049 Madrid, Spain
‡Dep. Chemistry and CNISM, Univ. of Rome La Sapienza, Piazzale A. Moro 5, 00185 Rome, Italy / Inst. Ion Physics, Univ. of Innsbruck, Innsbruck, Austria
§email: g.delgado@csic.es

INTRODUCTION

In recent investigations the feasibility of two He-Ca potentials has been tested for He_2Ca clusters by means of a variety of quantum mechanical (QM) methods[1,2]. The potential by Kleinekathöfer[3] (hereafter P1) and that by Lovallo and Klobukowski[4] (hereafter P2) differ on both the values of the equilibrium distance and of the well depth: ~ 7 Å and ~ 10 cm^{-1} for the P1 potential and ~ 8 Å and ~ 3.5 cm^{-1} for the P2 potential respectively. Besides the differences observed for both the number of bound states supported by each potential and the corresponding energies, simulated microwave spectra were found to exhibit remarkably distinct features. Thus, whereas the spectrum obtained when the much weaker P2 potential is employed simply reduces to one R_{00} and one P_{01} lines (for $L = 1$, $v' = 0 \leftarrow L = 0, v = 0$ and $L = 0$, $v' = 1 \leftarrow L = 1, v = 0$ transitions respectively, being L the total angular momentum and v the vibrational quantum number), for the P1 potential a more ample variety of possible transition lines is seen. In addition the calculation of the radial distributions for such clusters revealed interesting properties depending on whether ^{4}He or ^{3}He was considered since for $^4He_2Ca$, the two He atoms are located closer to each other than to the Ca atom, which was not the case for the fermionic cluster $^3He_2Ca$.

The specific position of the chromophore for aggregates formed with a larger number of He atoms is a subject of interesting investigations. In general, for atom doped helium clusters, this information is usually inferred by comparison between the corresponding electronic absorption spectrum and the measurements in the gas-phase or bulk situations. The shift and width of the electronic transitions constitute fairly good indicators about the cluster structure and the situation of the embedded species, which in turn has been found to depend on the intrisic nature of the atom bonded to the helium media. Thus, Ag[5] gets trapped inside the cluster while alkaline atoms such as Li, Na or K[6,7] remain at a dimple on the helium cluster's surface. For alkaline earth atoms, due to their interaction with He, predictions regarding the preferred location, either at the surface or inmersed in the bulk, are found to be in principle more uncertain. Mg, for example, constitutes an interesting borderline case between surface location and solvation[8,9]. Spectra of Ca[10], Sr[10], and Ba[11] attached to helium droplets are on the other hand much broader blue-shifted than those for alkalis. This

could be then interpreted as an indication of the inmmersion or formation of a bubble state inside the clusters[12]. Since the blue shift is smaller when the comparison is established with the corresponding spectra in the bulk helium, it has been suggested that the location of the impurity atoms could be in region of low helium density close to the surface of the droplet.

A crucial aspect which needs to be taken into consideration for these systems is the interaction between the dopant and the impurity. Based on the well depth and the equilibrium internuclear distance of the He-impurity potential, among other quantities, Ancilotto *et al.*[13] developed a simplistic model in which according with the value of a dimensionless λ parameter, it is in principle possible to predict whether or not a specific dopant is expected to be solvated in He. As shown by Reho *et al.*[8] different potential energy surfaces for He–Mg and He–Ca lead to different conclusions with values of λ both larger or smaller than the solvation threshold $\lambda_0 = 1.9$. In particular, for the combination between Ca and He, a SCF/CI potential[14] produces $\lambda = 2.1$ and the above mentioned P1 potential[3] yields a more favourable situation for solvation with $\lambda = 5.5$. However the HFD potential calculated in Ref.[8] predicts a value of λ which in principle corresponds to a non-solvation situation: $\lambda = 1.4$. As revealed in recent works, some other factors such as the existence of quantized vortices within the helium cluster[15,16] or the presence of an additional dopant as an Ar atom[17,18], can bring the Ca atom inside the droplet.

Despite the caution exhibited in order to extract definitive conclusions from the measured absortion spectra of Ca atoms attached to He clusters[10,12], the blue shift of ~ 70 cm^{-1} observed with respect the Ca $4s4p\,^1P_1 \leftarrow 4s^2\,^1S_0$ transition[10,19] have been usually interpreted as an indication of the surface location of the Ca atom. Therefore some of the most attractive He-Ca interaction potentials, such as the one reported in Ref.[3], have been commonly discarded in favour of some others[4,20] for which the model by Ancilotto *et al.*[13] seems to predict a surface location. However even with those potentials density functional calculations found that the difference between the minimum energy configuration, a stable dimple state at the surface of ^{4}He clusters, and the solvated state with the Ca impurity at the center of the cluster does not exceed ~ 10 cm^{-1}[21] for $N = 300 - 1000$ He atoms, certainly a small value in comparison with the energy associated to the absortion spectrum of the calcium atoms, $\sim 23600 - 23700$ cm^{-1}.

Calculations of the electronic excitation spectrum of Ca atoms attached to helium clusters have been reported for both ^{4}He[15] and ^{4}He-^{3}He mixtures[19,22]. Such theoretical simulations require of the electronically excited $^1\Pi$ and $^1\Sigma$ He–Ca interaction potentials[14,23] in addition to the ground $X^1\Sigma$ He–Ca interaction. In particular, possible inaccuracies in the potential obtained in Ref.[15] were invoked to explain the underestimation of about 25 cm^{-1} of the measured bulk liquid spectra[19]. The importance of the precise ratio between ^{3}He and ^{4}He for systems formed by a Ca atom attached to a mixed helium nanodroplets has been the subject of a recent series of theoretical studies[19,21,22]. In those investigations the calcium atom was found to be completely solvated in pure ^{3}He clusters but the behaviour differs in mixed ^{3}He-^{4}He samples. If the system is composed by the appropiate number of atoms of each isotope, it is possible to observe how the impurity penetrates the fermionic shell down to the ^{4}He core. In some way the above mentioned results for $^4He_2Ca$ and $^3He_2Ca$[2] suggest certain propensity, even for trimers, of the observed tendency of the Ca atom for larger clusters to occupy an outer dimple when the helium medium is made mainly of ^{4}He instead of ^{3}He.

In this work we extend our previous investigations on the He_2Ca trimers[1,2] by considering a larger number of He atoms. The energies and structures of He_NCa clusters with up to $N = 40$ ^{4}He atoms are analyzed as a function of the temperature by means of path integral Monte Carlo (PIMC) calculations. The issue of a possible different behaviour of the Ca impurity with respect to the surrounding He medium for these intermediate clusters is analyzed employing the above mentioned P1 and P2 potentials.

The structure of the paper is as follows: In the Theory section details on the theoretical method and on the present calculation are given; results are presented on the Results section and discussed on the Discussion section. Finally conclusions are listed in the Conclusions section.

THEORY

Path Integral Monte Carlo

The PIMC method employed in the present study has already been described before[24–27] so here we will restrict to its basic details. In the framework of this approach the density matrix at a temperature T, $\rho(R, R'; \beta) = \langle R'|e^{-\beta\hat{H}}|R\rangle$ employed to estimate the thermal average of a quantum observable $\hat{A}$ as:

$$\hat{A} = Z^{-1} \int dR dR' \rho(R, R'; \beta) \langle R|\hat{A}|R'\rangle, \tag{1}$$

is represented as the product of M density matrices at a higher-temperature $T' = T \times M$ as follows:

$$\begin{aligned} \rho(R_0, R_M; \beta) = & \int \dots \int dR_1 dR_2 \dots dR_{M-1} \rho(R_0, R_1; \tau) \\ & \times \quad \rho(R_1, R_2; \tau) \dots \rho(R_{M-1}, R_M; \tau) \end{aligned} \tag{2}$$

where R_α contains the position vectors of the N He atoms and the Ca atom at the time *slice* α, Z is the partition function and $\beta = 1/k_B T$. If M is finite we can define a discrete-time path as $\tau = \beta/M$, the *time step* of the path integral. Each density matrix of Eq. (2), $\rho(R_k, R_{k+1}; \tau)$, can be approximated based upon the Trotter formula[28]:

$$\rho(R_k, R_{k+1}; \tau) \approx \int dR' \langle R_k|e^{-\tau\hat{K}}|R'\rangle \langle R'|e^{-\tau\hat{V}}|R_{k+1}\rangle. \tag{3}$$

In this approximation the particles may be considered as moving freely with a small correction due to the presence of the potential $V(R)$. The symmetrization of the density matrix due to the bosonic character of the ^{4}He atoms has not been taken into account, a procedure which is valid in the present study given that the values of the temperature under consideration are sufficiently high[29].

The total Hamiltonian $\hat{H}$ for the present case is written as follows:

$$\begin{aligned} \hat{H} \quad = \quad & -\frac{\hbar^2}{2m_{\mathrm{Ca}}} \nabla^2_{\mathrm{Ca}} - \frac{\hbar^2}{2m_{\mathrm{He}}} \sum_{i=1}^{N} \nabla_i^2 + \sum_{i=1}^{N} V_{\mathrm{He-Ca}}(r_i) \\ + \quad & \sum_{i<j} V_{\mathrm{He-He}}(r_{ij}), \end{aligned} \tag{4}$$

where m_{He} is the helium atom mass, m_{Ca} is the calcium atom mass, derivatives in ∇^2_{Ca} are performed with respect to the Ca atom position vector, r_i is the distance between the i-th He and the Ca atom and r_{ij} are helium-helium distances.

For the PIMC calculation, we have chosen the so-called *thermodynamic* estimator by Baker[30], expressed as:

$$E_T = \frac{3(N+1)}{2\tau} - \left\langle \sum_{\alpha=1}^{M} \frac{(R_\alpha - R_{\alpha-1})^2}{4\lambda_m \tau^2} + \frac{1}{M}\sum_{\alpha=1}^{M} V(R_\alpha) \right\rangle \tag{5}$$

with $\lambda_m = \hbar^2/2m$, m being m_{Ca} or m_{He} depending on whether the specific position vector included in R refers either to the Ca atom or to any of the He atoms. In Eq. (5) $\langle\rangle$ means averaging over the Monte Carlo (MC) steps. The first term stands for the classical kinetic energy $(3/2)(N+1)k_BT$ multiplied by the number of beads and the last term contains the classical potential energy. The main advantage of this energy estimator for the present study in comparison with other choices (as the virial estimator employed for example on previous works on the He_NCs_2[29] and He_NRb_2[27] systems) is that one is not forced to evaluate derivatives of the dopant-impurity potential, a specially demanding task in terms of computational time in some cases such as the P1 potential.

The number of beads considered in the PIMC calculation varies between 30 and 450, an upper limit which was found to be enough on previous applications of the PIMC method on this kind of molecules[27]. After 10^7-10^8 steps in the MC calculation, the average energy for each He_NCa system considered here is finally obtained by extrapolating τ to 0 (or equivalently M to ∞) in a similar manner as done in some other previous calculations[31,32] according with a parabolic law. This method slightly differs however with the procedure employed in Ref.[27] where the energy was calculated as an average over the stable region of the function $E = E(M)$. We have tested that values of the energy obtained do not depend on the specific computation method. Error bars, on the other hand are more sensitive to these numerical details, and exhibit much smaller values when the above mentioned extrapolation is used.

The PIMC calculations have been performed with confinements imposed on the space available for the free displacements of the atoms constituing the system. Thus the evaporation of the helium atoms has been prevented by confining them inside a sphere centered at the Ca atom with a radius of 30 Å, and with distances between the center of mass (CM)

of the He droplet and the impurity limited to a maximum value of 15 Å. Smallest clusters, $N = 10$, at the lowest values of the temperature, $T = 1$ K, have been treated using other values of such confinements: 24 Å for the sphere surronding the Ca atom and 12 Å for the distance He CM-Ca atom. These values do not affect however the results obtained for the energy of the bound states.

In this work radial and angular distributions have been calculated in order to get some insight about the structure of the clusters. Distributions in terms of the distance between the Ca atom and any of the N He atoms are obtained as follows:

$$D_N(r) = \frac{1}{NM} \left\langle \sum_{\alpha=1}^{M} \sum_{i=1}^{N} \delta(r - r_i^{(\alpha)}) \right\rangle \tag{6}$$

where $r_i^{(\alpha)}$ is the distance between the $i-$th He and Ca atoms at the time *slice* α. Analogously, we have calculated distributions for $\cos\gamma$, γ being the angle formed by any pair of vectors joining the Ca atom to a pair of He atoms, $k \neq l$, $\mathbf{r}_k$ and $\mathbf{r}_l$:

$$D_N(\cos\gamma) = \mathcal{N} \left\langle \sum_{\alpha=1}^{M} \sum_{k<l}^{N} \delta(\cos\gamma - \hat{\mathbf{r}}_k^{(\alpha)} \cdot \hat{\mathbf{r}}_l^{(\alpha)}) \right\rangle \tag{7}$$

where the factor $\mathcal{N} = 2\left[N(N-1)M\right]^{-1}$ ensures that the distribution is normalized to 1 and $\hat{\mathbf{r}}_k^{(\alpha)} = \mathbf{r}_k^{(\alpha)}/r_k^{(\alpha)}$.

Pair Potentials

As already mentioned in the Introduction, in Eq. (4) for $V_{\mathrm{He-Ca}}(\vec{r_i})$ we have used the P1 potential by Kleinekathöfer[3] and the P2 potential by Lovallo and Klobukowski[4]. The $V_{\mathrm{He-He}}(r_{ij})$ interaction was described using the potential by Aziz and Slaman[33].

The two He–Ca potentials compared here are intrinsically different. On the one hand, the P1 potential is calculated within the framework of the Tang-Toennies model[34] and is fitted to the analytical form:

$$V(r) = D\exp(-b_1 r - b_2 r^2) + V_{\mathrm{disp}}(r) \tag{8}$$

with $D = 3.19\,E_h$, $b_1 = 1.05$ a$_0^{-1}$, $b_2 = 0.00745$ a$_0^{-2}$ and in which the long-range potential $V_{\rm disp}$ is described by the dispersion series:

$$V_{\rm disp}(r) = -\sum_{n\geq 3}^{5} f_{2n}(b'(r), r)\frac{C_{2n}}{r^{2n}}, \tag{9}$$

where the dispersion coefficients, $C_6 = 46.8\,E_h$ a$_0^6$, $C_8 = 1835\,E_h$ a$_0^8$ and $C_{10} = 118500\,E_h$ a$_0^{10}$ are taken from Ref.[35], and the damping functions $f_{2n}(b'(r), r)$ are calculated as:

$$f_{2n}(b'(r), r) = \left(1 - e^{-rb'(r)}\sum_{k=0}^{2n}\frac{(rb'(r))^k}{k!}\right), \tag{10}$$

with $b'(r) = b_1 + 2b_2 r$, as defined in Refs.[3,36].

The P2 potential[4] however has been obtained by means of *ab initio* calculations, in particular a well-tempered model core potential method. Coupled-cluster level of theory with single and double excitations and a perturbational treatment of the triple excitations were employed by Lovallo and Klobukowski[4] in the series of pair potentials between He and Group 2 elements. López-Durán *et al.*[2] fitted the *ab initio* points between 2 Å and 16.0 Å by means of the following expression:

$$\begin{aligned} V(r) &= Ae^{-kr}/r \quad r \leq r_0 \\ &= \sum_{n=3}^{7} c_{2n}/r^{2n} \quad r \geq r_0 \end{aligned} \tag{11}$$

where $r_0 = 4.6$ Å, $A = 2040362.862$ cm^{-1} Å, $k = 2.088$ Å^{-1}, $c_6 = 231619.170$ cm^{-1} Å^6 , $c_8 = 15438995.509$ cm^{-1} Å^8 , $c_{10} = 2085441484.937$ cm^{-1} Å^{10} , $c_{12} = 82383199752.866$ cm^{-1} Å^{12} and $c_{14} = 852545635932.049$ cm^{-1} Å^{14}.

RESULTS

PIMC calculations were performed for both the P1 and P2 He–Ca potentials to study systems formed with a different number of He atoms. The smallest size consisted of systems with $N = 10$ He atoms and the largest clusters contained $N = 40$ He atoms. We first focus on the energy of the bound states supported by the different aggregates over a temperature

range from $T = 1$ K to 2 K. Then the geometrical structure of the clusters for each He–Ca interaction will be discussed.

Energy

Given the distinct features of the P1 and P2 potentials already mentioned in the Introduction, energies of the He_NCa systems are expected to depend on the specific He–Ca potential employed in the PIMC calculation. Values of the energies for N =10, 20, 30 and 40 helium atoms at $T = 1$, 1.5 and 2 K are shown in Table 1. The actual value of the energy for those cases in which the result is above the total fragmentation threshold, i.e. positive, are not specified in the Table. For such situations the corresponding radial distributions are found to exhibit clear indications of delocalization which is only partially controlled by the artificial confinements imposed on the PIMC calculation. We find that, for each specific number of He atoms, N, the difference between the results obtained with the P1 potential ($E_{\rm P1}$) and those for the P2 potential ($E_{\rm P2}$) increases with the temperature.

Despite the fact that the present application of the PIMC is restricted to values of the temperature larger than 1 K, an estimate of the energies when $T \to 0$ can be obtained by using instead a diffusion Monte Carlo (DMC) calculation. In order to do so, we have employed the same DMC approach as in previous investigations[2,29,37,38]. Thus, for $He_{10}Ca$, values of -44.80 and -12.25 cm^{-1} for the P1 and P2 He–Ca potentials, respectively, are predicted. The corresponding DMC estimates for $He_{20}Ca$ are -96.23 cm^{-1} and -33.65 cm^{-1}, respectively. These DMC energies are found to correlate quite well with the PIMC results at finite temperature, as revealed by global least mean square fittings to an analytical expression such as $a_1 + a_2 e^{T/a_3}$. In fact, a similar procedure for the DMC and PIMC results reported by Boronat *et al.*[39] for pure He_N clusters shows a similar correlation.

An important aspect in the energetics of this sort of doped clusters is to investigate their possible stability in comparison with the energies of the pure He_N clusters formed with the same number of He atoms. If the He droplet is capable to form a stable complex with the Ca impurity, one would expect its energy, $E(He_NCa)$, to remain below $E(He_N)$, the energy of the pure He bound state. Fig. 1 shows the comparison between the results reported by Boronat *et al.*[39] for He_N clusters and the present PIMC energies for the Ca-doped aggregates

obtained with the P1 potential for the He–Ca interaction. The values for the He_NCa clusters with $N = 20$ and 40 are clearly below the energies of the corresponding pure He systems for this potential. Whereas the He_N clusters end up with energies above the fragmentation threshold, that is become positive, for $T > 1.25$ K, the He_{20}Ca and He_{40}Ca systems look perfectly stable.

The situation is noticeably different when the P2 He–Ca potential is employed in the PIMC calculation. The energies shown in Fig. 2 reveal that the stability of He_{20}Ca and He_{40}Ca in terms of the comparison with the He_{20} and He_{40} systems is a delicate issue. With the error bars (see Figs. 1 and 2) associated to the energies it is not straightforward to conclude that such systems support bound states with no fragmentation or evaporation of the Ca atoms with respect to the He droplet.

A remarkable feature observed for $N = 40$ at $T = 2$ K is the stability of the He_{40}Ca droplet in comparison with the corresponding pure He_{40} cluster which exhibits a positive binding energy. The addition of the impurity thus introduces some glue effect which gathers the surrounding helium atoms into a stable structure around the Ca atom for both the P1 and P2 potentials employed in this work.

Structure

A first indication on the geometrical structures of the clusters can be obtained by looking at the beads describing the Ca and He atoms of the PIMC simulation. In the upper panels of Fig. 3 snapshots of the simulations for He_{10}Ca at $T = 1$ K reveal differences in the structure of the clusters depending on the potential employed to describe the interaction between dopant and solvent. Whereas for the P1 interaction the Ca atom seems to be partially surrounded by He atoms, the situation for the P2 potential corresponds to the onset of a small cavity inside the He cloud to host the Ca atom. When the number of He atoms is increased to $N = 40$ (see bottom panels of Fig. 3) the impurity gets solvated when the P1 He–Ca interaction is employed. However, the added He atoms to the system described by the much weaker P2 potential preserve the dimple structure in which the Ca atom finally locates. This latter result seems to be consistent with the situation predicted by experimental observations[10]. Thus, the remarkable differences in the energies between the bound states of

the $He_N Ca$ systems obtained for each He–Ca potential correlate with a noticeably distinct positionings of the impurity with respect to the helium droplet.

The structure of the clusters is further analyzed by means of probability densities in terms of the corresponding internal distances and angles. In particular, following Eq. (7) we have calculated the probability density $D(\cos\gamma)$ and Fig. 4 shows the result for $He_{40}Ca$ at $T = 1$ K. Each He–Ca potential yields a different geometry for the doped cluster. Thus, the cluster seems to stabilize according to an almost completely isotropic structure when the P1 potential is employed in the calculation; $\cos\gamma \sim 1$ constitutes the only exception since $D(\cos\gamma)$ displays a minimum about that specific direction. This isotropy is consistent, as shown in Fig. 3, with a Ca atom solvated by the He cloud, a situation in which equiprobability should be expected for the angle formed by any two He–Ca bonds.

On the contrary, the densities for the P2 potential, shown in Fig. 4, manifest a marked preference for $\cos\gamma \sim 1$ with a non negligible probability down to $\cos\gamma \sim 0.5$. The corresponding angular range, $\pi/4 > \gamma > 0$, can be interpreted as being the most probable when the Ca impurity, installed inside the dimple (see right bottom panel of Fig. 3), does not have an entire shell of He atoms over it as compared with the case with a full solvating environment.

Extra support for the solvation versus dimple-structure comparison is found when we analyze radial distributions obtained for each He–Ca potential. For example, the density functions in terms of the distance between the Ca atom and the CM for the He cloud, shown for $N = 40$ and $T = 1$ K at Figs. 5 and 6, display Lorentzian-type profiles with maximum peaks at distinct values depending on the potential. Thus, the result for the calculation performed with the P1 potential has its maximum around ~ 1.5 Å, a much smaller distance than the corresponding maximum observed for the P2 potential, ~ 9 Å.

The short distance between the Ca atom and the CM of the He droplet in combination with the profile of the $D_{40}(r)$ function for the probability density as a function of the He–Ca distance (shown in red dashed line in Fig. 5) describe a situation, for the cluster with the P1 He–Ca interaction, in which the Ca atom is not strictly at the center (1.5 Å away from it) of the solvating structure formed by the He atoms, mainly located at a ~ 5.5 Å distance. The helium cage around the Ca atom is not enterely a sphere, with an extra shell-like He band

~ 8 Å away from the Ca atom. Whether or not this is the result of the limited number of He atoms considered for this work and if the impurity would finally locate at the center of the cluster for $N \gg 40$ remain as open questions to be solved on larger systems.

Analogously, for the P2 potential, the maximum peak at ~ 9 Å, and a probability for the $D_{40}(r)$ function as shown in Fig. 6 (in red dashed line) reveals that the Ca atom sees sorrounding He atoms at both larger and shorter distances than the corresponding distance to the He CM. The above mentioned dimple is thus consistent with this structure of He atoms at different distances with respect to the impurity: The shortest He–Ca distances being for He atoms at the surface of the cavity which hosts the impurity, and the largest He–Ca distances describing He atoms which are at the completely opposite location.

Figs. 5 and 6 also show the He–Ca probability densities for a smaller doped cluster, $He_{10}Ca$ (in black solid lines). The comparison with the case in which $N = 40$ reveals for the P1 potential, for instance, an almost spherical geometry around the Ca atom, as shown in the more pronounced maximum at $r \sim 5.5$ Å of the corresponding distribution shown in Fig. 5. The tail of the distribution does not extend as much as the cluster with a larger number of He atoms. The addition of more He atoms to the cluster with the P2 He–Ca potential also leads to significant differences in the geometrical location of He around the Ca impurity. As already manifested in Fig. 3, the He atoms find enough space to locate preferentially at $r \sim 7$ Å away from the Ca atom (see the maximum in Fig. 6) and with a smaller probability, to distances up to almost 14 Å. However, with $N = 40$ atoms different relative maxima are found for the distance which separates the impurity and the He atoms.

Another interesting feature to note from the $D_N(r)$ probability densities of Figs. 5 and 6 is the effects of the distinct features of the He–Ca interactions analyzed in this work. Whereas both $He_{10}Ca$ and $He_{40}Ca$ clusters present distributions which do not go further away by more than 11 Å for the P1 potential, for the considerably weaker P2 interaction, the distances between Ca and He can reach easily 18 Å.

Probability densities for the He–He distance are also included in Figs. 5 and 6 for the $He_{40}Ca$ clusters at $T = 1$ K (black dotted lines). No significant differences are observed when the He–Ca potential is changed. The number of He atoms does not produce noticeable effects either on the average profile shown by the corresponding radial probabilities in Figs

5 and 6 apart of a slight decrease in the corresponding He–He distance when we consider $N = 10$. The maximum found around 9-10 Å and the corresponding average distance, $\langle r_{ij} \rangle$, of about 9.3 Å, are larger than the thermal wave lenght of the system at $T = 1$ K, ~ 8.7 Å, thus supporting the possibility of a not explicit inclusion of the exchange permutation symmetry for the helium atoms in the PIMC approach[40]. In this sense, recent calculations on $He_{64}Na^+$ and $He_{64}Mg^+$ clusters performed with a similar PIMC treatment yielded radial distributions at $T = 1$ K which were almost identical to those obtained when the exchange symmetry is properly taken into account[41].

DISCUSSION

The comparative study of two He–Ca potentials proposed here reveals the relevance of a correct description of the impurity–dopant interaction. For the present case there is an ample number of potentials available on the literature, where recent examples correspond to either models developed via semi empirical formulations such as the presently employed P1 potential, that based on the Tang-Toennies potential model[42] and that previously reported by Stienkemeier *et al.*[43], or to QM *ab initio* calculations. Within this latter group one can find the already mentioned SCF/CI potential by Czuchaj *et al.*[14] or its renewed version[23], the HFD potential by Reho *et al.*[8], the accurate QM studies of Hinde[20] and the CCSD(T) P2 potentials employed in this work. Each of these two sets of potentials manifest marked differences regarding the well depth and the minimum equilibrium distance. Thus, P1 and P2 somewhat represent examples of each of these two families. An interesting comparison between the CCSD(T) potentials and those estimated from semi empirical models can be established for the entire rare gas-Ca interactions, by means of the results from Refs.[23] and[42]. In these two works, potentials between Ca and Xe, Kr, Ar, Ne and He were developed. Well depths were found to increase with the mass of the corresponding rare gas atoms in both works. Equilibrium distances, R_e, on the contrary follow an opposite trend for both type of calculations: whereas for the CCSD(T) potentials (with the only exception of Xe) R_e was found to increase from Kr (5.05 Å) to He (5.85 Å), Yang *et al.*[42] found that the equilibrium distances decrease, being the He–Ca interaction the one with the smallest

equilibrium distance (4.93 Å) of the series.

In this sense it is worth mentioning that the model proposed in the study of the physics of solvation by Ancilotto and coworkers[13] to establish whether or not a specific He–impurity interaction leads to a solvating structure predicts, for P2 and the rest of potentials belonging to the last family, a solvated-Ca structure. The value of the λ parameter as defined in Ref.[13] is ~ 2 for these interactions: as computed by Hernando *et al.*[21], λ varies between 2.04 for the P2 potential and 2.49 for the newer version of the potential by Czuchaj *et al.*[14]. $He_N Ca$ systems are therefore borderline cases in which λ slightly exceeds the threshold for solvation λ_0 and should then lead to clusters in which the impurity remains solvated inside a cage structure formed by the He atoms. On the contrary present PIMC results for the P2 potential and those reported in Ref.[21] for Hinde's potential[20] clearly indicate that the predicted geometry is quite the opposite. These situations in which the value of λ remains within a certain window around the λ_0 threshold are extremely dependent on the precise details of the potential[20,21]. The limitation on the validity of Ancilotto *et al.* model for the title system can be due to different factors. First, the original formulation was established for Lennard-Jones type potentials and secondly no dependence with the temperature is contained in the value of the λ parameter which determines the behaviour predicted for the solvant.

Previous investigations on the Ar_3 system[26] included a comparative analysis between results obtained by means of the PIMC method in its QM version ($M > 1$) and those obtained within a classical version $M = 1$. The presence of a large number of He atoms in the present clusters discards such an approach in this study. In fact, as shown in Fig. 7 for $He_{40}Ca$ at $T = 1$ K, no solvation is predicted for the P1 He-Ca potential under classical assumptions.

The differences with the QM PIMC results for the P1 potential can be explained in terms of the behaviour of the global interaction inside the doped cluster following a classical picture. The He–Ca potential has an equilibrium distance which is much larger than the corresponding He–He one. Within a classical regime, the average energy of the system is mainly ruled by the total interaction, which, whatever the relations between the potential depths, obeys the following behaviour:

$$V \sim N \times V_{\mathrm{He-Ca}} + 0.5 \times N(N-1)V_{\mathrm{He-He}}. \quad (12)$$

Therefore Eq. (12) means that the contribution from the He–Ca interaction grows linearly with N whereas the contribution from He–He goes quadratically. Thus the helium atoms tend to cluster together away from the Ca dopant thereby preventing its solvation. This behaviour is even more pronounced as N increases, so larger clusters are expected not to solvate the Ca impurity. It is by invoking a QM picture and including zero energy point effects that the description gets complete and solvation, depending on the character of the He–Ca interaction, can take place.

A remarkable feature observed for the case of the He–Ca P1 potential is that, according to the situation shown in the snapshot of Fig. 3, the solvation is not complete and the impurity can be seen through a small cavity in the environing helium atoms. This is consistent on the other hand with the fact that the Ca atom is not exactly located on the CM of the cluster but some short distance away, surely as a result of the observed anisotropy induced by the absence of interacting He atoms along the direction pointing towards the hole open in the surrounding helium cloud. These sort of considerations regarding the precise location of embbeded species are of relevance for instance when the refrigerating properties of helium are investigated. It is at the center of the droplet where the active cooling of the dopant by helium atoms evaporation gets more efficient[44]. The reason for this partial solvation might be that the number of helium atoms N considered in this work is not large enough. Sizes in some other previous works vary between a couple of hundreds[16] up to a couple of thousands helium atoms[15,21], but the comparison with present results for the solvating case is hindered by the fact that: (i) results reported in those studies were obtained with a much weaker He–Ca potential than the P1 one and (ii) the temperature was not included in such studies. It is only by means of a quantized vortex that the Ca atom is dragged down to the center of the cluster[16]. However even for those potentials, in which the impurity remains at the surface, it is found that the depht of the dimple which hosts the Ca atom increases with N[15,21], thus suggesting a much more profound location inside the He droplet. The extreme case of such a dependence with the number of He atoms has been found for Mg impurities in helium droplets, in which the location of the impurity shifts from a surface to a bulk state

as He atoms are added to the cluster[9,45].

The stability of the He_NCa systems studied here has been analysed in terms of the corresponding pure He_N clusters. Since a great deal of interest is usually manifested in the energetics and dynamics of doped clusters when the number of He atoms is modified[21,46–49], we clearly see in Figs. 1 and 2 the binding energy of the doped clusters increases with N. Therefore the evaporation or ejection of the He atoms from the He_NCa system at a constant value of T has to be understood as a loss of stability of the entire cluster. The energy release as the He atoms leave can be estimated from the PIMC values shown in Table 1. According with the present results for the P1 He–Ca potential the loss of 10 He atoms involves an energy loss $\Delta E_{10}^{(N)} = E(He_NCa) - E(He_{N-10}Ca)$ which can vary between 50-10 cm^{-1} and which is found to decrease with T and N. The only exceptions to this apparent rule have their origin in the energies obtained for the $He_{30}Ca$ system at T =1.5 and 2 K which lead to a different trend for $\Delta E_{10}^{(40)}$ and $\Delta E_{10}^{(30)}$.

The helium droplets of the experimental studies reported on Refs.[10,19] are formed at nozzle temperatures ranging between 10 K and 15 K. Once the Ca impurities are solvated by means of the pick-up technique[50], the rapid evaporation of the helium atoms reduces the temperature of the clusters[51]. We have considered in this work values for T between 1 K and 2 K, consistent with those reported in the laser spectroscopic investigation by Moriwaki and Morita[52] in which Ca atoms are inmmersed into liquid ^{4}He kept at $T = 1.4$ K. We therefore investigate the He_NCa systems at slightly larger values than the rotational temperatures inferred for impurities embedded in large superfluid helium clusters, ~ 0.4 K[53,54]. However our present results confirm the stability of the Ca-doped helium aggregates up to $T = 2$ K even for the weakest He-Ca interaction potential here employed when $N = 40$.

Cooling of the helium droplets after evaporation of atoms from the cluster has been studied theoretically before by means of different models[48,49]. In Ref.[49] variations of the energy and temperature of the system as the helium atoms depart were monitored in terms of the evaporation time according to a statistical rate model which includes the total angular momentum conservation. The evaporative cooling trajectories shown in that work involve a decrease of both T and the internal energy accompanying the loss of the helium atoms. That is also the behaviour expected from the energy curves as a function of the temperature shown

in Figs. 1 and 2. According to those figures for example the evaporation of a specific number of He atoms keeping the internal energy of the clusters $He_N Ca$ unchanged would also require a decrease of the value of the temperature, ΔT, as a consequence of the thermal-kinetic energy released with the departing atoms. The precise value of this temperature-energy release seems to depend on the initial conditions of the process, and the evaporation of a specific number of atoms might lead to different results depending on the size of the droplet and the value of the initial temperature.

CONCLUSIONS

The $He_N Ca$ clusters with $N = 10 - 40$ at different values of the temperature, 1, 1.5 and 2 K, have been studied by means of PIMC calculations. For the theoretical simulations two different He–Ca potentials have been compared, the one by Kleinekathöfer[3] (P1) and the potential proposed by Lovallo and Klobukowski[4] (P2). The main differences between these two potentials show up in their equilibrium distance and well depth values, with about 6 cm^{-1} difference between both cases. The stronger interaction, the P1 potential, yields energies for the doped clusters which are clearly below the corresponding pure He_N droplets, thus indicating their stability with respect to a possible fragmentation or ejection of the Ca atom, whereas a similar comparison for the energies obtained with the P2 potential reveals that such stability is a more uncertain and delicate issue.

The structure of the title system depends on the nunmber of He atoms and dramatically on which He–Ca potential is employed in the PIMC calculation. While the P1 potential leads to the solvation of the Ca impurity within a cage formed by the He atoms, the much weaker P2 interaction produces a structure for the cluster in which the Ca atom locates in a dimple formed by the more external atoms of the He surface, a finding consistent with the experimental information reported in the literature for the $He_N Ca$ aggregates.

ACKNOWLEDGMENTS

This work has been supported by MICINN Grant No. FIS2011-29596-C02-01. R.R.-C and D.L.-D. also acknowledge support by Grant No. JAE-Pre-2010-01277 and JAE-DOC,

Contract No. E-28-2009-0448699, respectively. One of us (FAG) further acknowledges the support of the PRIN 2009 Research Project by the Italian MIUR.

References

1. López-Durán, D.; Rodríguez-Cantano, R.; González-Lezana, T.; Delgado-Barrio, G.; Villarreal, P.; Gianturco, F. A. *Phys. Rev. A* **2012**, *86*, 022501.
2. López-Durán, D.; Rodríguez-Cantano, R.; González-Lezana, T.; Delgado-Barrio, G.; Villarreal, P.; Gianturco, F. A. *Eur. Phy. J. D* **2012**, *66*, 1.
3. Kleinekathöfer, U. *Chem. Phys. Lett.* **2000**, *324*, 403.
4. Lovallo, C. C.; Klobukowski, M. *J. Chem. Phys.* **2004**, *120*, 246.
5. Bartelt, A.; Close, J. D.; Federmann, F.; Quaas, N.; Toennies, J. P. *Phys. Rev. Lett.* **1996**, *77*, 3525.
6. Nakayama, A.; Yamashita, K. *J. Chem. Phys.* **2001**, *114*, 780.
7. Bartelt, A.; Close, J. D.; Federmann, F.; Hoffman, K.; Quaas, N.; Toennies, J. P. *Z. Phys. D: At. Mol. Clusters* **1997**, *1*, 1.
8. Reho, J.; Merker, U.; Radcliff, M. R.; Lehmann, K. K.; Scoles, G. *J. Chem. Phys.* **2000**, *112*, 8409.
9. Navarro, J.; Mateo, D.; Barranco, M.; Sarsa, A. *J. Chem. Phys.* **2012**, *136*, 054301.
10. Stienkemeier, F.; Meier, F.; Lutz, H. O. *J. Chem. Phys.* **1997**, *107*, 10816.
11. Stienkemeier, F.; Meier, F.; Lutz, H. O. *Eur. Phys. J. D* **1999**, *9*, 313.
12. Stienkemeier, F.; Vilesov, A. F. *J. Chem. Phys.* **2001**, *115*, 10119.
13. Ancilotto, F.; Lerner, P.; Cole, M. *J. Low Temp. Phys.* **1995**, *101*, 1123.
14. Czuchaj, E.; Rebentrost, F.; Stoll, H.; Preuss, H. *Chem. Phys. Lett.* **1991**, *182*, 191.
15. Hernando, A.; Barranco, M.; Mayol, R.; Pi, M.; Krośnicki, M. *Phys. Rev. B* **2008**, *77*, 024513.
16. Ancilotto, F.; Barranco, M.; Pi, M. *Phys. Rev. Lett.* **2003**, *91*, 105302.

17. Hernando, A.; Masson, A.; Briant, M.; Mestdagh, J. M.; Gaveau, M. A.; Halberstadt, N. *J. Chem. Phys.* **2012**, *137*, 184311,

18. Masson, A.; Briant, M.; Hernando, A.; Halberstadt, N.; Mestdagh, J. M.; Gaveau, M. A. *J. Chem. Phys.* **2012**, *137*, 184310.

19. Bünermann, O.; Dvorak, M.; Stienkemeier, F.; Hernando, A.; Mayol, R.; Pi, M.; Barranco, M.; Ancilotto, F. *Phys. Rev. B* **2009**, *79*, 214511.

20. Hinde, R. J. *J. Phys. B: Atom. Mol. Opt. Phys.* **2003**, *36*, 3119.

21. Hernando, A.; Mayol, R.; Pi, M.; Barranco, M.; Ancilotto, F.; Bünermann, O.; Stienkemeier, F. *J. Phys. Chem. A* **2007**, *111*, 7303.

22. Guardiola, R.; Navarro, J.; Mateo, D.; Barranco, M. *J. Chem. Phys.* **2009**, *131*, 174110.

23. Czuchaj, E.; Krośnicki, M.; Stoll, H. *Chem. Phys.* **2003**, *292*, 101.

24. Ceperley, D. M. *Rev. Mod. Phys.* **1995**, *67*, 279.

25. Kwon, Y.; Ceperley, D. M.; Whaley, K. B. *J. Chem. Phys.* **1996**, *104*, 2341.

26. Pérez de Tudela, R.; Marquez-Mijares, M.; González-Lezana, T.; Roncero, O.;Miret-Artés, S.; Delgado-Barrio, G.; Villarreal, P. *J. Chem. Phys.* **2010**, *132*, 244303.

27. Rodríguez-Cantano, R.; López-Durán, D.; Pérez de Tudela, R.; González-Lezana, T.; Delgado-Barrio, G.; Villarreal, P.; Gianturco, F. A. *Comp. Theor. Chem.* **2012**, *990*, 106.

28. Trotter, H. F. *Proc. American Math. Soc.* **1959**, *10*, 545.

29. Pérez de Tudela, R.; López-Durán, D.; González-Lezana, T.; Delgado-Barrio, G.; Villarreal, P.; Gianturco, F. A.; Yurtsever, E. *J. Phys. Chem. A* **2011**, *115*, 6892.

30. Barker, J. A. *J. Chem. Phys.* **1979**, *70*, 2914.

31. Cuervo, J. E.; Roy, P.-N. *J. Chem. Phys.* **2006**, *125*, 124314.

32. Blinov, N.; Song, X.; Roy, P.-N. *J. Chem. Phys.* **2004**, *120*, 5916.

33. Aziz, R. A.; Slaman, M. J. *J. Chem. Phys.* **1991**, *94*, 8047.

34. Tang, K. T.; Toennies, J. P. *J. Chem. Phys.* **1984**, *80*, 3726–3741.

35. Standard, J. M.; Certain, P. R. *J. Chem. Phys.* **1985**, *83*, 3002–3008.

36. Tang, K. T.; Toennies, J. P *Surface Science Letters* **1992**, *279*, L203–L206.

37. Rodríguez-Cantano, R.; López-Durán, D.; González-Lezana, T.; Delgado-Barrio, G.; Villarreal, P.; Yurtsever, E.; Gianturco, F. A. *J. Phys. Chem. A* **2012**, *116*, 2394.

38. López-Durán, D.; Rodríguez-Cantano, R.; González-Lezana, T.; Delgado-Barrio, G.; Villarreal, P.; Yurtsever, E.; Gianturco, F. A. *J. Phys. Cond. Matt.* **2012**, *24*, 104014.

39. Boronat, J.; Sakkos, K.; Sola, E.; Casulleras, J. *J. Low Temp. Phys.* **2007**, *148*, 845–849.

40. Ceperley, D. M.; Pollock, E. L. *Phys. Rev. Lett.* **1986**, *56*, 351–354.

41. Galli, D. E.; Ceperley, D. M.; Reatto, L. *J. Phys. Chem. A* **2011**, *115*, 7300–7309.

42. Yang, D. D.; Li, P.; Tang, K. T. *J. Chem. Phys.* **2009**, *131*, 154301.

43. Stienkemeier, F.; Meier, K.; Stark, K.; Lutz, H. *Farad. Discuss.* **1997**, *108*, 212.

44. Bonhommeau, D.; Lewerenz, M.; Halberstadt, N. *J. Chem. Phys.* **2008**, *128*, 054302.

45. Mella, M.; Calderoni, G.; Cargnoni, F. *J. Chem. Phys.* **2005**, *123*, 054328.

46. Guillon, G.; Zanchet, A.; Leino, M.; Viel, A.; Zillich, R. E. *J. Phys. Chem. A* **2011**, *115*, 6918.

47. Loginov, E.; Drabbels, M. *J. Chem. Phys.* **2012**, *136*, 154302.

48. Brink, D. M.; Stringari, S. *Z. Phys. D* **1990**, *15*, 257.

49. Lehmann, K. K.; Dokter, A. M. *Phys. Rev. Lett.* **2004**, *92*, 173401.

50. Gough, T. E.; Mengel, M.; Rowntree, P. A.; Scoles, G. *J. Chem. Phys.* **1985**, *83*, 4958.

51. Stienkemeier, F.; Higgins, J.; Ernst, W. E.; Scoles, G. *Z. Phys. B* **1995**, *98*, 413.

52. Moriwaki, Y.; Morita, N. *Eur. Phys. J. D* **2005**, *33*, 323.

53. Hartmann, M.; Miller, R. E.; Toennies, J. P.; Vilesov, A. *Phys. Rev. Lett.* **1995**, *75*, 1566.

54. Stienkemeier, F.; Higgins, J.; Ernst, W. E.; Scoles, G. *Phys. Rev. Lett.* **1995**, *74*, 3592.

Figure 1: Energies of the $He_N Ca$ clusters, with $N = 20$ and 40, calculated with the P1 potential[3] for the He–Ca interaction in comparison with the energies of the pure He_{20} and He_{40} systems as reported in Ref.[39].

Figure 2: Same as Fig. 1 using the P2 potential[4] for the He–Ca interaction in the case of the $He_N Ca$ systems.

Figure 3: Snapshots from the PIMC calculation for $He_N Ca$ systems at $T = 1$ K with the P1 potential for the He–Ca interaction[3] (left panels) and with the P2 potential[4] (right panels). Upper panels are for $N = 10$ and bottom panels are for $N = 40$. Beads for the Ca atom are in green and those for the He atoms are in white.

Figure 4: Angular distributions in $\cos\gamma$ (see Eq. (7)) obtained with the P1 and P2 He–Ca potentials for $He_{40}Ca$ at $T = 1$ K, where γ is the angle formed between two vectors joining Ca–He atoms. See text for details.

Figure 5: Radial distributions as a function of the distance bewteen the Ca atom and any He atom (see Eq. (6)) for the P1 He–Ca potential for $He_{10}Ca$ (black solid line) and $He_{40}Ca$ (red dashed line) at $T = 1$ K. The probability density for the distance between the Ca atom and the CM of the He cluster (blue dashed-dotted line) and for the He–He distance (black dotted line) for $N = 40$ at $T = 1$ K are also included .

Figure 6: Same as Fig. 5 for the P2 potential for the He–Ca interaction.

Figure 7: Snapshot as in Fig. 3 obtained from the PIMC simulation in its clasic version, $M = 1$, for the $He_{40}Ca$ system at $T = 1$ K with the P1 potential for the He–Ca interaction..

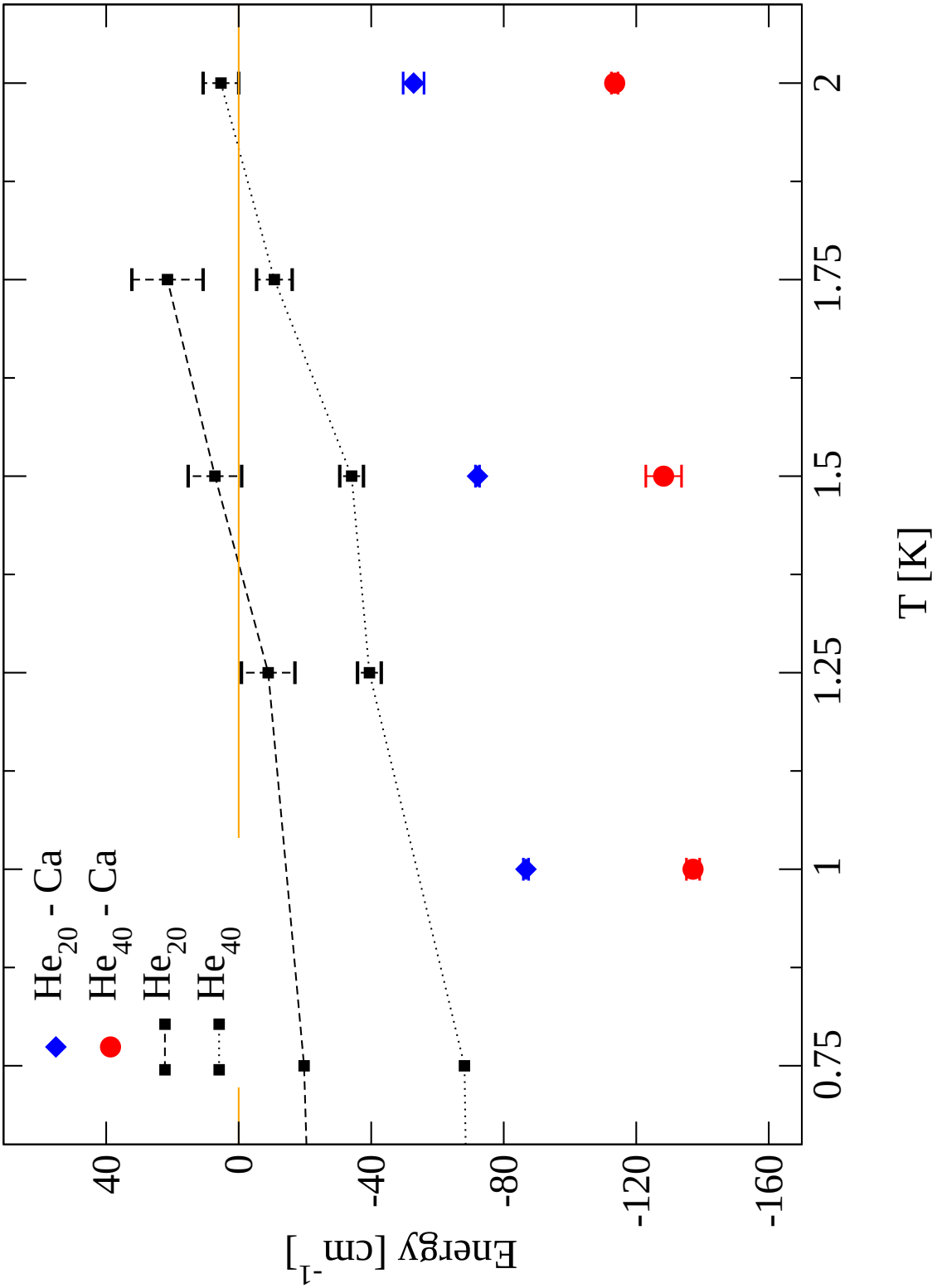
Energy [cm-1]
40
0
-40
-80
-120
-160
T [K]
0.75
1
1.25
1.5
1.75
2
He20 - Ca
He40 - Ca
He20
He40

Figure 1
R. Rodríguez-Cantano, *et al.*
Int. J. Quant. Chem.

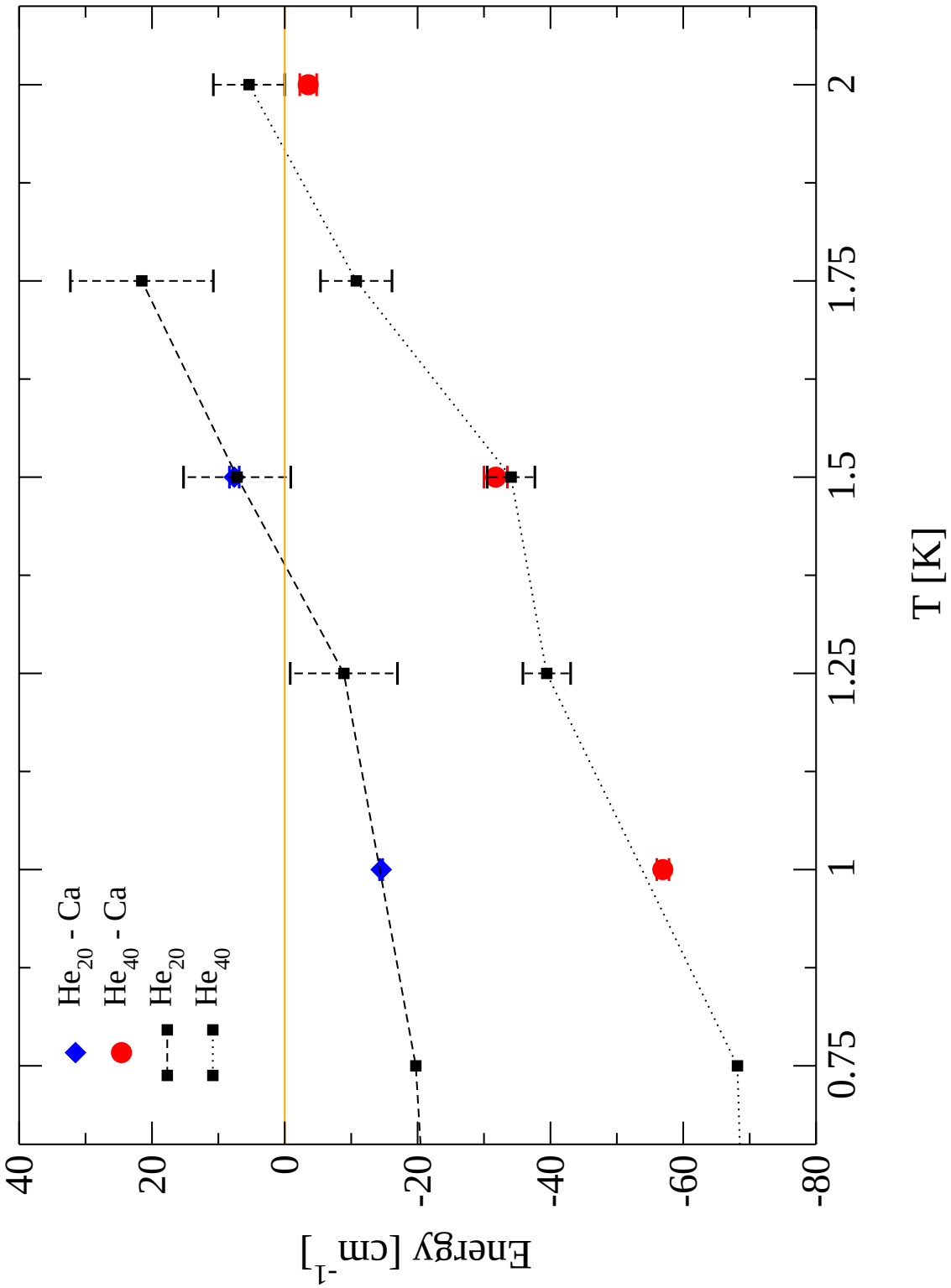
Energy [cm-1]
40
20
0
-20
-40
-60
-80
T [K]
0.75
1
1.25
1.5
1.75
2
He20 - Ca
He40 - Ca
He20
He40

Figure 2
R. Rodríguez-Cantano *et al.*
Int. J. Quant. Chem.

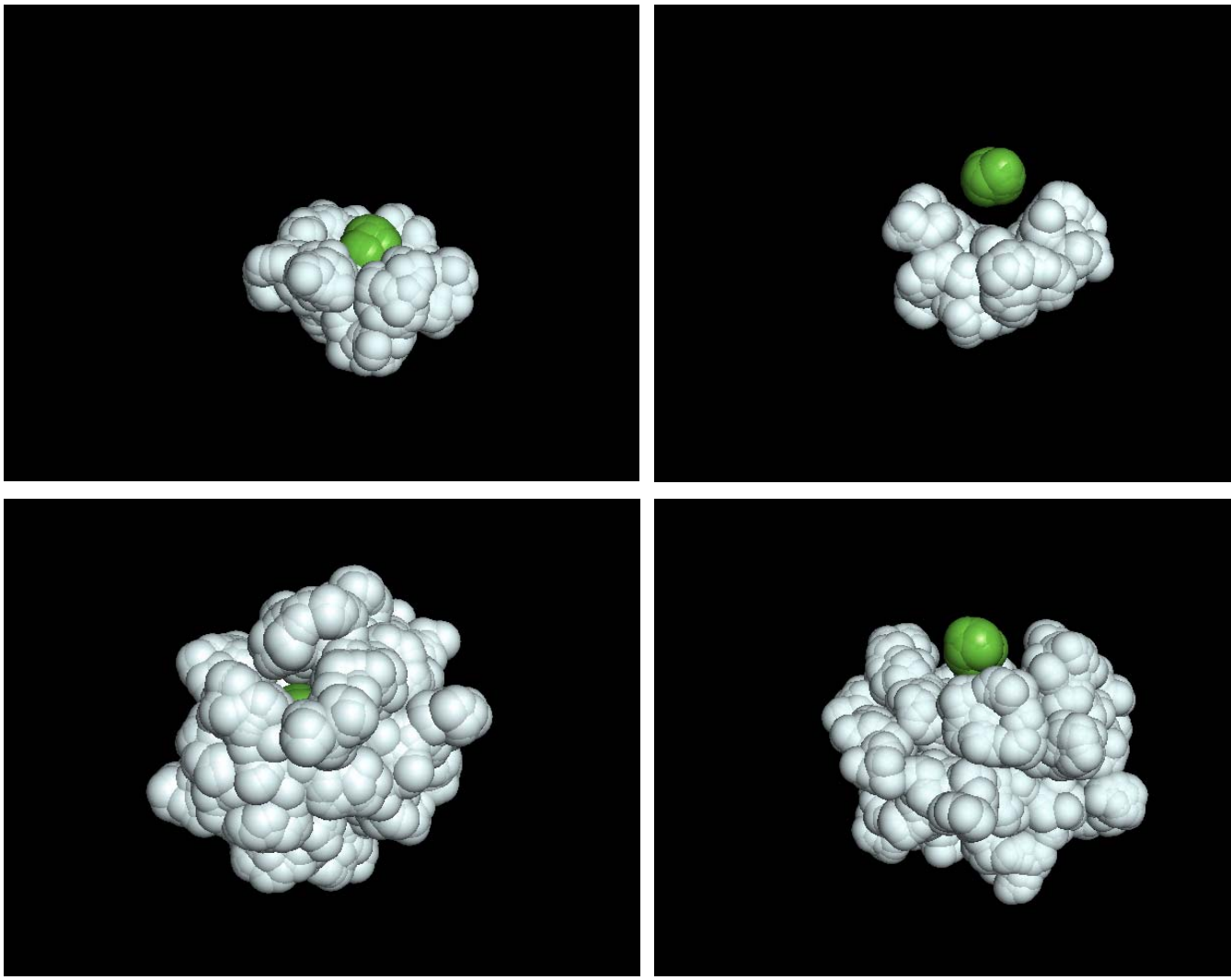

Figure 3
R. Rodríguez-Cantano *et al.*
Int. J. Quant. Chem.

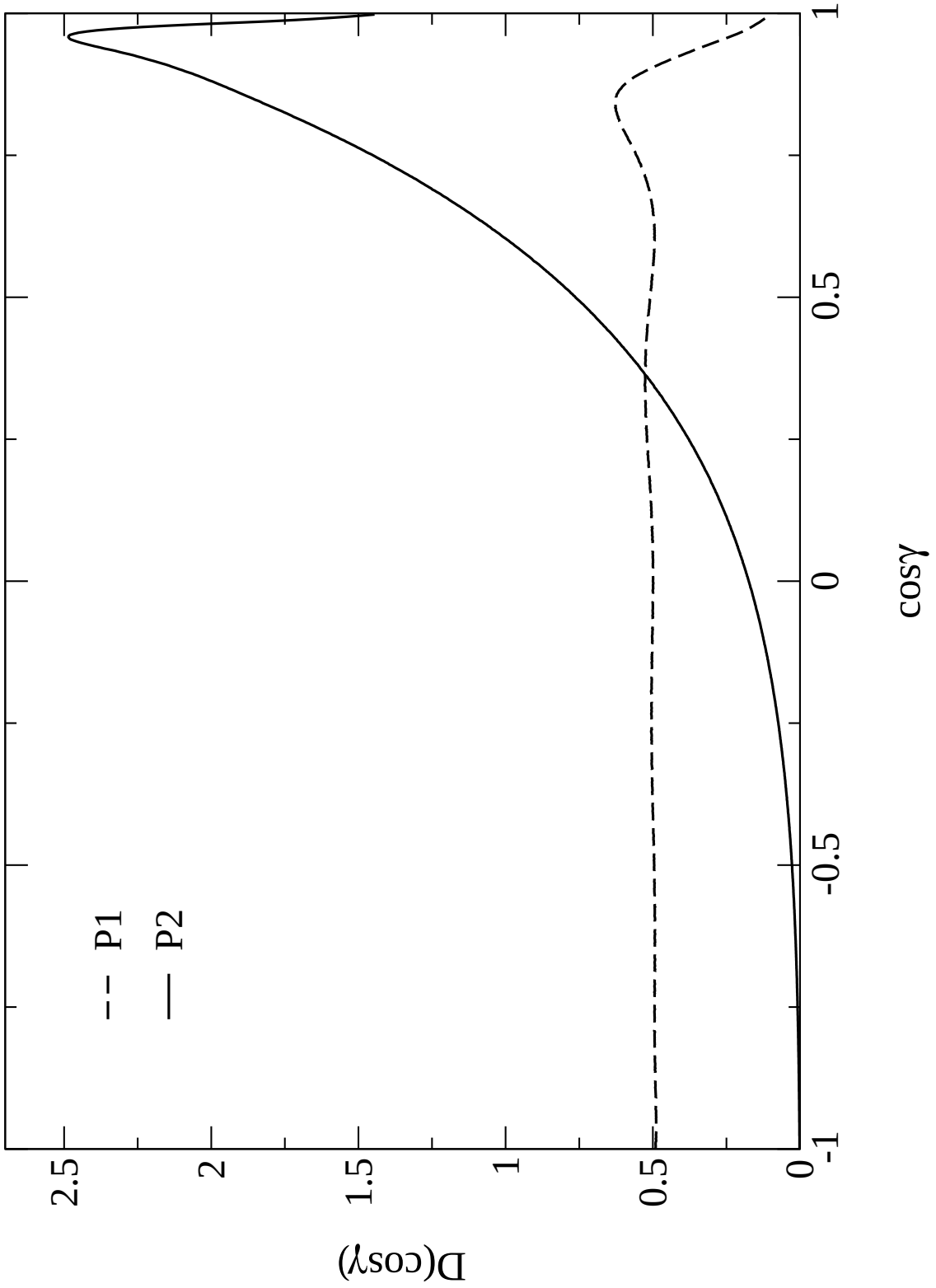
D(cosγ)
cosγ
P1
P2
2.5
2
1.5
1
0.5
0
1
0.5
0
-0.5
-1

Figure 4
R. Rodríguez-Cantano *et al.*
Int. J. Quant. Chem.

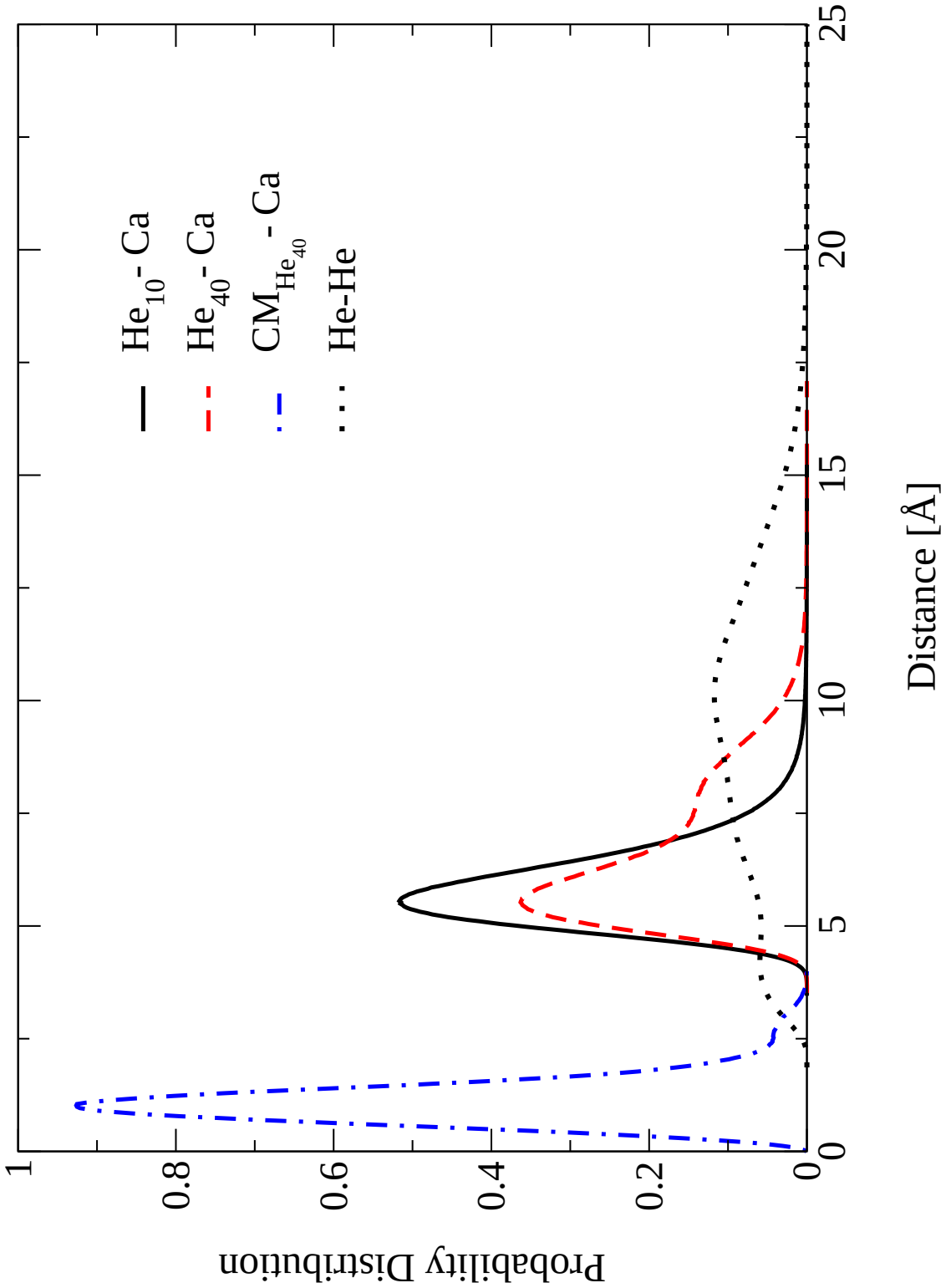
Probability Distribution
Distance [Å]
0
0.2
0.4
0.6
0.8
1
0
5
10
15
20
25
He_{10}- Ca
He_{40}- Ca
$CM_{He_{40}}$ - Ca
He-He

Figure 5
R. Rodríguez-Cantano *et al.*
Int. J. Quant. Chem.

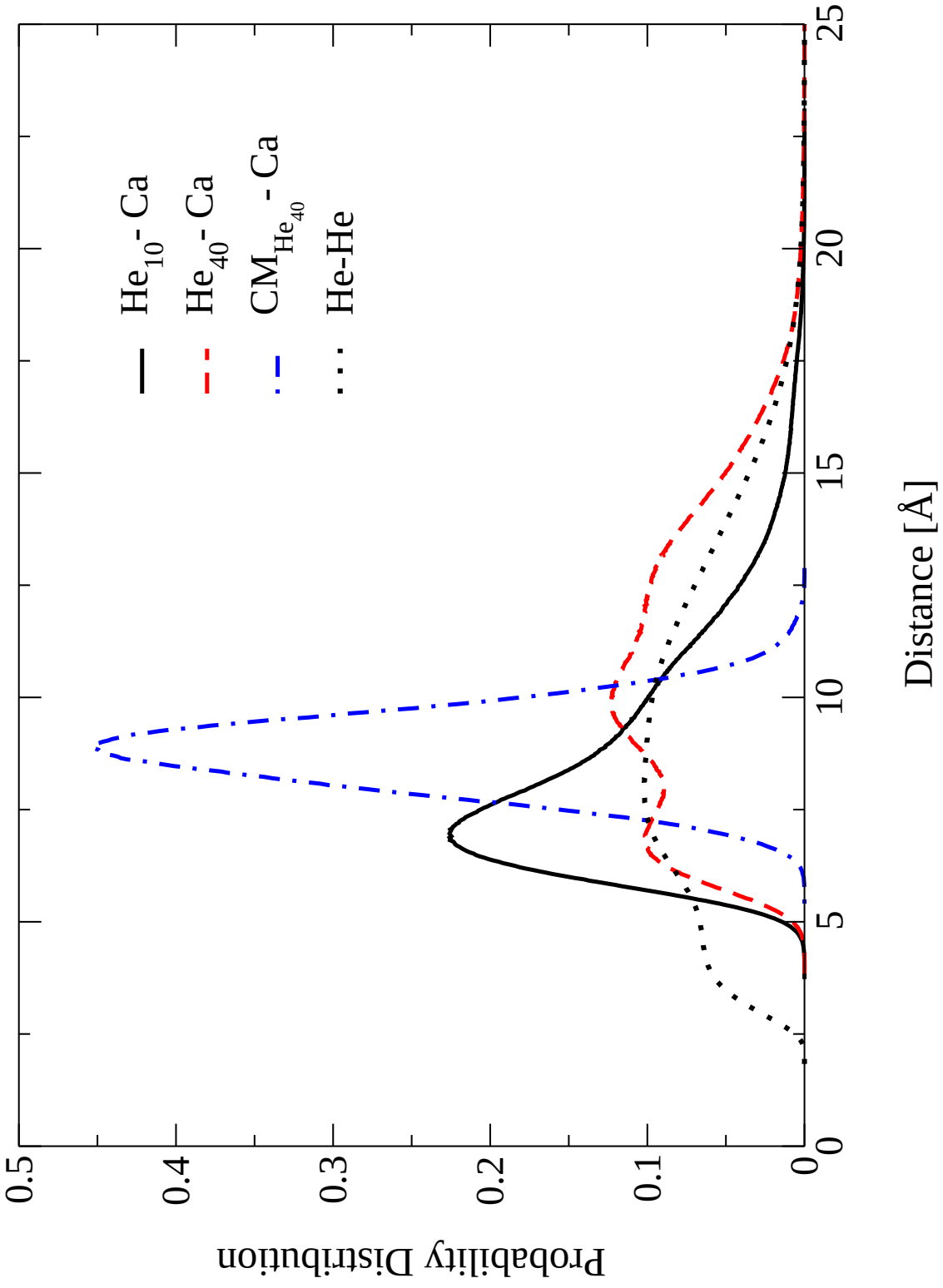
Probability Distribution
0.5
0.4
0.3
0.2
0.1
0
0
5
10
15
20
25
Distance [Å]
He10 - Ca
He40 - Ca
CMHe40 - Ca
He-He

Figure 6
R. Rodríguez-Cantano *et al.*
Int. J. Quant. Chem.

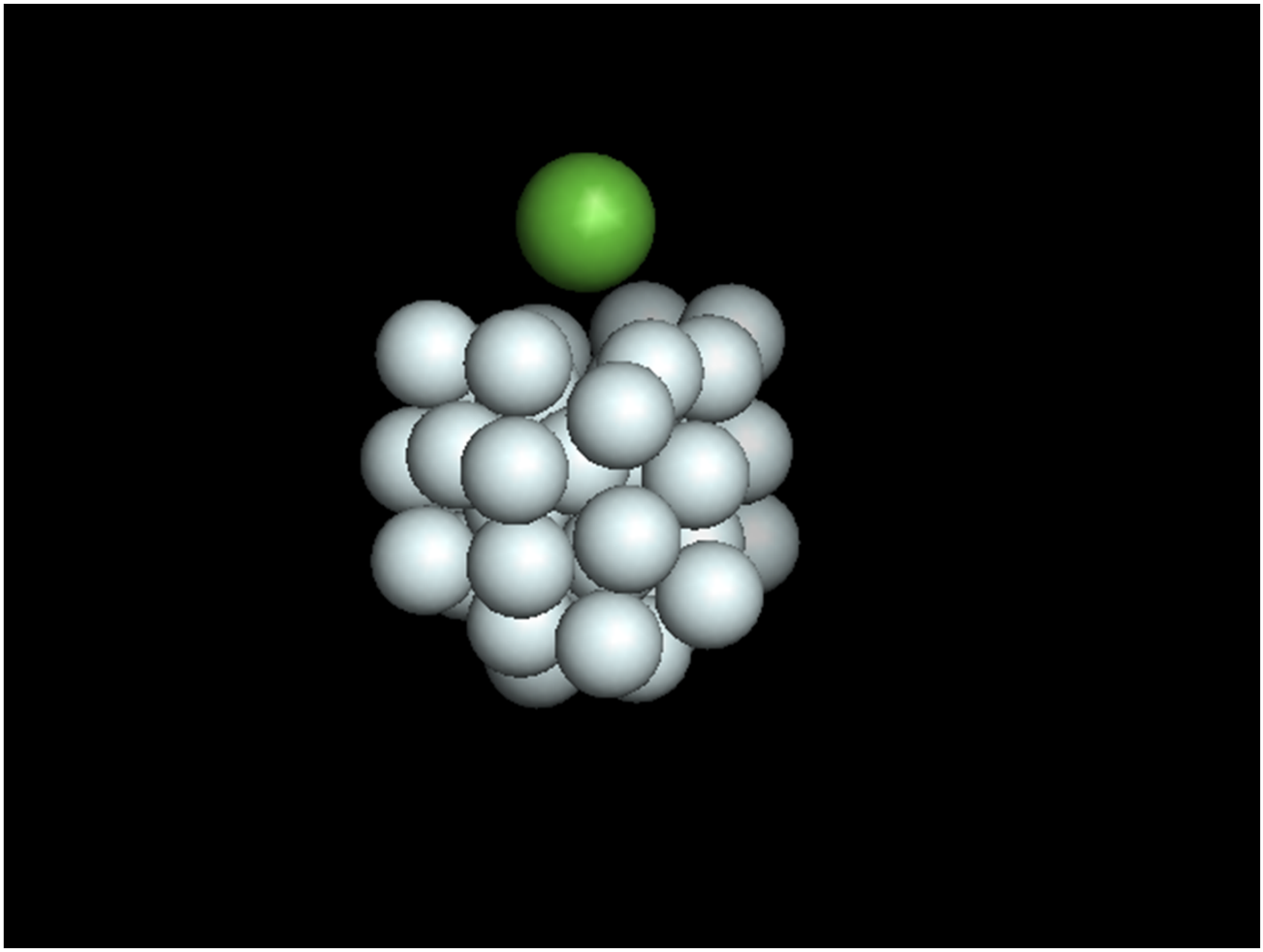

Figure 7
R. Rodríguez-Cantano *et al.*
Int. J. Quant. Chem.

Potential	$E(T = 1\,\mathrm{K})$	$E(T = 1.5\,\mathrm{K})$	$E(T = 2\,\mathrm{K})$
$N = 10$			
P2	-2.67	> 0	> 0
P1	-38.60	-32.12	-24.65
$N = 20$			
P2	-14.51	> 0	> 0
P1	-86.71	-72.08	-52.79
$N = 30$			
P2	-30.21	-11.74	> 0
P1	-118.97	-109.75	-71.85
$N = 40$			
P2	-56.93	-31.76	-3.52
P1	-137.16	-128.28	-113.50

Table 1: Energies (in cm^{-1}) at $T = 1$, 1.5 and 2 K of the $\mathrm{He}_N\mathrm{Ca}$ systems studied in this work with the P1[3] and P2[4] He–Ca potentials .

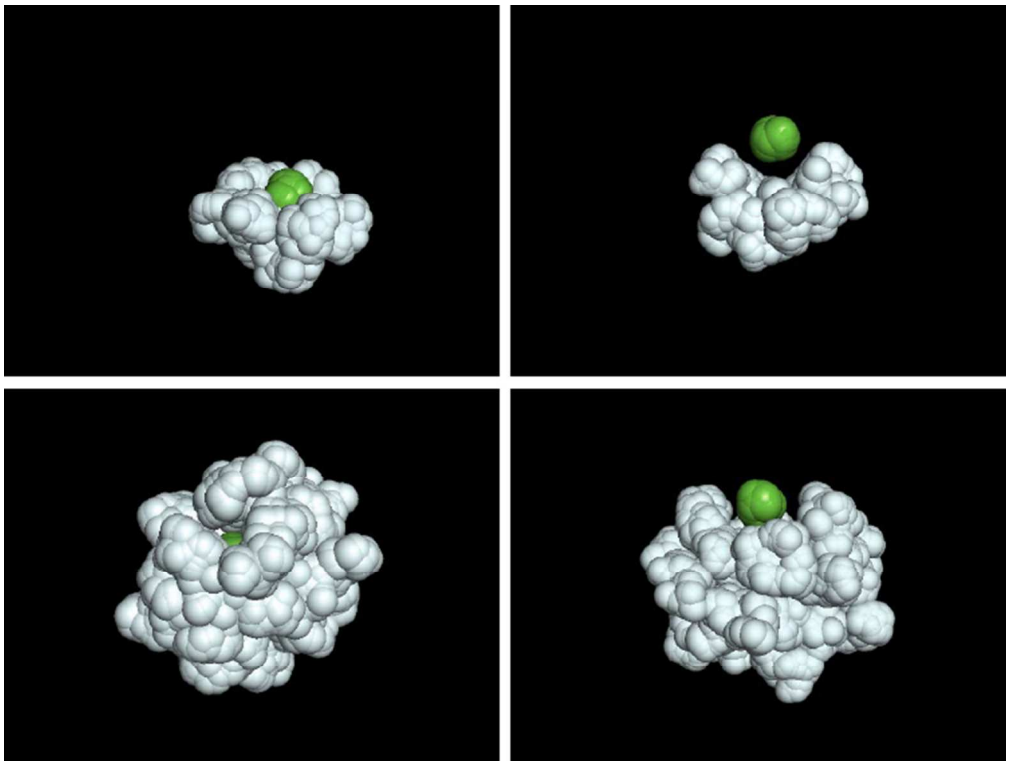

The precise location of Ca impurities in He droplets is investigated by means of path integral Monte Carlo calculations for clusters with up to 40 He atoms. The structure and energetics depends on the He-Ca interaction employed. This article discusses the issue in detail in comparison with existing experimental results
197x149mm (96 x 96 DPI)